Published by Nigerian Society of Physical Sciences. Hosted by FLAYOO Publishing House LTD

Proceedings of the Nigerian Society of Physical Sciences

Journal Homepage: https://flayoophl.com/journals/index.php/pnspsc

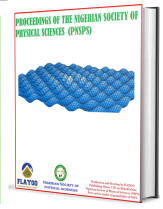

High performance multilayer satellite electronic shielding system (MULSES)

Lubem James Utume[a,*], Abubakar Sadiq Aliyu[a], Abdulkarim Muhammad Hamza[a], Muhammad Sani[a], Umar Sa'ad Aliyu[a], Mngusuur Scholastica Iorshase[a], Emmanuel Ochoyo Adamu[a], Wasiu Oyeyemi Salami[b], Isaac Pada[c], Emmanuel Ogwuche[d]

[a]*Department of Physics, Faculty of Sciences, Federal University of Lafia, P. M. B 146, Lafia, Nasarawa State, Nigeria*
[b]*Department of Polymer Technology, Nigerian Institute of Leather and Science Technology, Zaria*
[c]*Department of Medical Physics National Hospital, Abuja*
[d]*Department of Science Laboratory and Technology, College of Environmental Sciences and Technology Makurdi, Benue State*

A B S T R A C T

Passive radiation shielding has gained prominence in space technology due to satellite malfunction and destruction by high-energy beta particles in low Earth orbit (LEO). This paper describes the synthesis and characterization of a novel composite material composed of aluminum oxide (Al_2O_3), hexagonal boron nitride (h-BN), and high-density polyethylene (HDPe) reinforced with Doum fiber. MULSES mechanical properties exhibited tensile strength of 25 MPa, hardness of 85.7 Hv, and impact energy absorption of 23.721 J, demonstrating a perfect combination of strength, flexibility, and toughness. Thermogravimetric analysis (TGA) showed the composite has thermal stability until approximately 600°C, degradation was initiated at 320°C and optimal degradation was at 480°C. Differential thermal analysis (DTA) showed peaks of exothermic degradation at 400°C and 520°C corresponding to decomposition of polymer and fibers, respectively, and show the suitability of the composite to handle high temperature. Radiation shielding efficiency was tested at various beta (6, 9, 10, 12, and 15 MeV) and gamma (662 keV and 1.25 MeV) energies. Stacking arrangement played a crucial role in shielding efficiency, with the BHA (Boron, HDPe, Aluminum) arrangement delivering the maximum beta radiation protection efficiency (RPE) of 99.16% at 6 MeV and 95.42% at 15 MeV. When compared to other stack arrangements, the BHA arrangement showed 12% improvement in beta attenuation efficiency and 8% improvement in gamma attenuation efficiency. The smaller mean free path (MFP) and half-value layer (HVL) for beta and gamma radiation also confirm the improved shielding property of the BHA arrangement. HDPe-Doum fiber-h-BN-Al_2O_3 exhibits the optimum mechanical strength, heat stability, and radiation shielding properties all together that render MULSES a cost-effective, light, and renewable space shielding material.

Keywords: Satellites, Space radiation, Linac, HDPe, Biomass.

DOI:10.61298/pnspsc.2025.2.168

1. INTRODUCTION

Satellites play a crucial role in modern communication, navigation, Earth observation, and scientific research. However, they are constantly being bombarded with high-energy cosmic radiation, which creates significant problems for their performance and lifespan. Space radiation consists primarily of Solar Particle

*Corresponding Author Tel. No.: +234-812-0443-571.
e-mail: utumelubem1010@gmail.com (Lubem James Utume)

Events (SPEs) and Galactic Cosmic Radiation (GCR). SPEs are recurring releases of high-energy electrons, protons, and heavy nuclei from solar flares and coronal mass ejections. By comparison, GCR is of supernova origin from outside our solar system and consists of protons, alpha particles, and heavy ions of high energy traveling at relativistic speeds with energies of more than 10GeV/nucleon [1, 2]. High-energy particles have the ability to penetrate deeply into spacecraft materials, producing deadly secondary radiation upon collision.

The interaction of GCR with spaceflight shielding materials generates secondary particles, including neutrons, which are significant in radiation-induced damage [3]. Secondary neutrons, formed through spallation reactions, pose a critical risk to electronic devices and biological tissue during space travel. Due to their deep penetration capability into materials, it is difficult to shield them, and thus advanced material designs are required for enhancing attenuation efficiency [4]. Unless adequately shielded, such radiation impacts would induce Single Event Effects (SEEs) through upsets, latch-ups, and burnouts in satellite electronics and long-term Total Ionizing Dose (TID) degradation, thus degrading mission reliability.

Aluminum and polyethylene, which are conventional shielding materials, have been used widely; they do have their limitations, though. Aluminum, while being structurally sound, produces secondary radiation when it comes into contact with high-energy particles, further worsening radiation exposure. Polyethylene is effective in hydrogen-based neutron shielding but lacks good mechanical and thermal properties for harsh space environments [5]. These shortcomings necessitate the development of more advanced shielding materials that possess greater radiation attenuation, mechanical strength, and thermal stability.

This study will develop a new multilayered composite material consisting of high-density polyethylene (HDPe), Doum fiber reinforcement, hexagonal boron nitride (h-BN), and aluminum oxide (Al_2O_3). Each material is selected on the basis of its individual characteristics that make an ideal shielding solution. HDPe possesses high hydrogen content and is therefore highly effective against neutron radiation with the added advantage of being lightweight. Doum fiber is introduced as a green reinforcement for the development of mechanical properties, thermal stability, and being a suitable replacement for man-made fibers. Hexagonal boron nitride (h-BN) is introduced due to its high thermal conductivity, oxidation resistance, and neutron absorption characteristics, which benefit space shielding applications. Aluminum oxide (Al_2O_3) ultimately enhances the structural stability of the composite and facilitates high-energy particle attenuation. Intermixture of such materials results in a synergism, improving overall shielding efficiency for the composite together with enhancing the mechanical toughness as well as heat stability.

This research endeavors to demonstrate the feasibility of such multi-functional composites as a low-cost and lightweight shielding material for space application. By utilizing a synergy of the inherent properties of each material, the study endeavors to improve satellite lifespan and performance in severe space conditions.

2. DESCRIPTION OF EXPERIMENTAL PROCEDURE

2.1. MATERIAL SELECTION

The selection of High-Density Polyethylene (HDPe), Doum fiber, hexagonal Boron Nitride (h-BN), and Aluminum Oxide (Al_2O_3) was driven by their excellent structural, mechanical, and shielding properties. HDPe was chosen because of its strength-to-weight ratio, radiation resistance, and ease of processing. Doum fiber was utilized as reinforcement owing to its richness in tensile strength, its biodegradability, and ability to strengthen impact resistance. Hexagonal Boron Nitride (h-BN) was incorporated due to its thermal stability, neutron-absorbing, and lubricant properties, assuring better mechanical behavior. Aluminum Oxide (Al_2O_3) was incorporated due to its high hardness, thermal conduction, radiation shielding efficiency, and space-mission suitability.

2.2. SYNTHESIS OF HDPE

The synthesis of doum reinforced HDPe began with the collection and preparation of raw materials, where Doum fiber was sourced and cleaned thoroughly, dried, and cut into 5mm equal pieces. The polymer matrix (HDPe) was preheated in a two-roll mill at 210°C, and the shredded leaves of doum palm was added incrementally, mixed, and sheeted out. This HDPe-Doum fiber composite was also subjected to hot pressing at 160°C and 2.5 MPa for 5 minutes, with subsequent cooling and cutting to standard test specimen sizes according to ASTM D638 (100mm × 10mm dumbbell shape) for tensile testing, ASTM D256 (100mm × 10mm) for impact testing, ASTM D2240 (100mm × 10mm) for hardness testing and 4cm × 4 cm for beta and gamma testing were subsequently done.

2.3. PREPARATION OF H-BN AND AL_2O_3

For homogeneity and optimal particle dispersion, h-BN and Al_2O_3 were fine-ground to have equal particle size (5μm) distribution before being mixed with an epoxy resin matrix. Epoxy resin (Epochem 105) and a hardener (Triethylene tetramine) were the matrix binders. The filler was mixed with the epoxy system using high-shear mixing with subsequent degassing to remove air bubbles. The homogenous blend was then cast into pre-prepared molds and cured under room temperature conditions for 24 hours. Sheets that were produced were trimmed to standard sizes according to ASTM D638 (100mm×10mm dumbbell shape) for tensile testing, ASTM D256 (100mm×10mm) for impact testing, ASTM D2240 (100mm × 10mm) for hardness testing (4cm × 4 cm) for beta and gamma testing were subsequently done.

2.4. FABRICATION OF MULSES

The multilayered shielding structure (MULSES) was prepared by combining the HDPe-Doum fiber, h-BN, and Al_2O_3 composite layers in a systematic manner. To ensure adhesion and prevent potential delamination issues, surfaces were cleaned using isopropyl alcohol and bonded with an acrylic adhesive. Acrylic adhesive was utilized since it has very good adhesive properties of high shear and peel strength and the ability to maintain structural integrity under mechanical and thermal stresses [6–8]. The layers were oriented in the desired orientations, and a 20 kg pressure was applied evenly for 12 hours for bonding. While adhesive strength tests were not conducted in this study, the adhesive was chosen based on its well-documented performance in high-

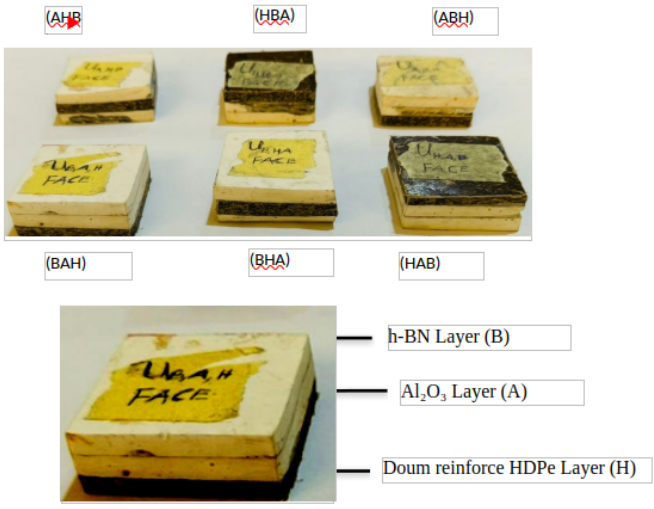

Figure 1. Six fabricated MULSES based on different surface orientation.

strength composite applications, ensuring the durability and reliability of the multilayered structure during operating conditions. Figure 1 shows all orientation of arrangements in the MULSES.

2.5. CHARACTERIZATION OF MULSES

2.5.1. Mechanical and physical characterization

Mechanical and thermal testing was performed, including tensile strength, impact strength, hardness, and thermogravimetric analysis (TGA).

The tensile strength was carried out in accordance with ASTM D-638. A dumbbell shaped samples were subjected to a tensile force and tensile strength, tensile modulus percentage elongation at break for each sample were calculated and recorded automatically by the machine and the results were on the certificate.

The impact test was carried out according to the standard specified ASTM $D^{-1}56$.The specimen was cut to dimensions 64mm × 12.7 mm × 3.2 mm and 45° notched was inserted at the middle of the test specimens from all the produced composite samples. The impact energy test was carried out using Izod Impact Tester (Resil impactor testing machine). The specimen was clamped vertically on the jaw of the machine and hammer of weight 1500N was released from an inclined angle 152°. The impact energy for corresponding tested specimen was taken and recorded.

The hardness test was carried out in accordance with ASTM D2240 on a MicoVicker Harness Tester. The test was carried out at different positions on each sample and average hardness was calculated.

2.5.2. Thermogravimetric analysis (TGA)

Thermogravimetric analysis (TGA) was performed using a Q5000 IR thermo-analyzer (TA Instruments) to determine the thermal stability of the samples and quantify their fraction of volatile components. The analysis involved monitoring the weight change of the samples during heating at a constant rate under nitrogen and air atmospheres. The instrument operated by continuously weighing the sample while heating, with an inert gas flowing over it. Gaseous by-products formed during the process were removed, and the changes in the remaining mass of the samples were recorded automatically. The samples were measured in an alumina crucible, with masses ranging from 11 to 18 mg. Composite samples were tested in an open platinum (Pt) pan over a temperature range of 25°C to 800°C, with a heating rate of 10°C/min.

2.5.3. Radiation shielding characterization

Radiation shielding performance was analyzed through beta and gamma-ray attenuation experiments. Beta attenuation testing was performed using the LINAC machine Elekta Synergy Platform 80 multileaf at different energies (6 MeV to 15 MeV). The fabricated multilayered materials with six (6) orientations were taken to Radiological unit, National Hospital Abuja, Nigeria for radiation shielding characterization.

Thermoluminescent dosimeters (TLDs) were annealed prior to the experiment to reset them for accurate dose measurements. The annealing process was conducted according to the manufacturer's guidelines using Pocket annealer (tension:230V 50Hz, Pmax:40W serial Number: annealer 2019).

The linear accelerator (Linac) was calibrated to generate electron beams at different energy levels: 6 MeV, 9 MeV, 10 MeV, 12 MeV, and 15 MeV. All safety protocols were strictly observed, and the experimental area was properly shielded to ensure safe operations. Background radiation levels were recorded using the annealed TLDs before starting the experiment to account for environmental radiation. These background readings were used for correction in subsequent measurements. To validate the accuracy of the TLDs, a TLD was positioned at a fixed distance from the Linac without any shielding material in the beam's path. The Linac was set to 15 MeV with a delivered dose of 1000mSv, and the transmitted dose was measured using the TLD. A fabricated material placed between the Linac and the TLD. The TLD was exposed to the transmitted dose (I), and the dose measurement was recorded using a TLD reader (model: microstar, serial number: 120771). The procedure was repeated for all six (6) orientations of the fabricated material at an energy level of 6 MeV, ensuring precise alignment for each measurement. After measurements at 6 MeV, the TLDs were read, annealed, and available for the subsequent energy level. The Linac energy was increased to 9 MeV, and the experiment was repeated for every orientation of the material formed. This was repeated for every energy level given: 6 MeV, 9 MeV, 10 MeV, 12 MeV, and 15 MeV. Background intensities of radiation were subtracted from all intensity measurements to obtain corrected values. The data were then computed according to the beta attenuation law in order to determine attenuation properties of the material produced.

For gamma-ray test shielding, point sources Co-60 and $Cs^{-1}37$ were employed. The experiment was carried out using a published method of our group [8] wherein the radiation intensity was read by a Geiger-Müller counter both before and after transmission through composite material.

3. RESULTS AND DISCUSSION

3.1. RESULTS FOR PHYSICAL AND MECHANICAL TEST

The physical characteristics of the MULSES show variation in thickness and density based on different orientation and layer stacking as shown in Table 1.

The thickness of the samples, as gauged, ranges between 1.495

Table 1. Result for physical test.

S/N	Orientation	Density (g/cm^3)	Thickness (cm)
1	BHA	1.7243±0.1345	1.525±0.0058
2	ABH	1.6867±0.0938	1.495±0.0058
3	HBA	1.8670±0.0744	1.555±0.0058
4	AHB	1.9263±0.1195	1.555±0.0058
5	BAH	2.0100±0.1350	1.5675±0.0050
6	HAB	1.8960±0.0773	1.545±0.0058

cm (ABH) and 1.5675 cm (BAH) with minimal variations across all the samples, the variations suggest some consistency in the manufacturing process but also indicate that there are material stacking orders that have an influence on the resultant thickness. Thickness inconsistency in composite shielding materials, based on Refs. [9, 10], can significantly influence their mechanical strength and radiation attenuation efficiency, where denser layers tend to contribute to enhanced shielding performance.

Density is a determining factor in how effective radiation shield materials are. The densities vary from 1.6867g/cm^3(ABH) to 2.0100g/cm^3 (BAH). More dense materials tend to have better attenuation of particles with high energies since they pack more atomic nuclei per volume unit [10]. The variations detected show that there are stacking orders that lead to more effective compaction and lower void content, which is indispensable for optimal shielding performance.

Denser samples (e.g., BAH, AHB, HAB) exhibit enhanced mechanical strength along with radiation attenuation due to the increased amount of high-density fillers like Aluminum Oxide (Al_2O_3) and hexagonal Boron Nitride (h-BN). Previous research studies indicate that multilayered shielding systems with high-density ceramics exhibit enhanced protection against gamma radiation [10].

Less dense samples (e.g., ABH, BHA): Reflect a larger degree of porosity or less dense packing, which can compromise mechanical integrity but reduce overall weight, an important factor for space applications. Studies of multilayer composite shielding have shown the significance of material selection and layer ordering on physical and shielding properties. For instance, Ref. [10] reported that ceramic filler-reinforced polymeric composite exhibited density-dependent shielding ability, which corroborated the findings in this research, where compositions of higher densities exhibited potentially improved shielding features. Similarly, Ref. [11] established that hybrid composites derived from the integration of Boron Nitride and Aluminum Oxide into polymer matrices provided enhanced mechanical and thermal stability, which aligned with the trends displayed in MULSES [12]. The reduction in thickness with a good density will help improve the space radiation shielding efficiency without sacrificing the mechanical strength. This is also consistent with what was observed in MULSES, where samples like BAH and AHB achieved relatively higher densities without large increases in thickness, indicating that there is a good balance between shielding performance and weight.

Mechanical property of the multilayer shield material was investigated through tensile, impact, and hardness testing as shown in Table 2 above. Tensile strength of the composite material was

Table 2. Results of mechanical characterization.

Test Type	Test Parameter	Value
Impact Test	Impact Strength (J)	23.721
Hardness Test	Hardness (Hv)	85.7
Tensile Test	Tensile Strength (MPa)	25

measured as 25 MPa, common for natural fiber-reinforced polymer composite material and close to ceramic-filled HDPe composites. Standard HDPe's tensile strengths fall between 20 MPa to 37 MPa and change with its molecular structure and the conditions for its processing [13]. Doum fiber addition enhances mechanical strength with minimal impact on flexibility, whereas h-BN and Al_2O_3 inclusion contributes to general structural reinforcement. Compared to conventional space-grade polymers like polyimides (50-$^{-1}$20 MPa) or PEEK-based composites (80-$^{-1}$00 MPa), the tensile strength of the composite material obtained is reduced; however, it is sufficient for non-load-bearing shielding purposes where impact resistance and thermal stability are greater concerns [14].

The composite impact energy, 23.721 J, suggests toughness, which is critical in space technology where the material to be shielded must withstand impacts from micrometeoroids and orbital debris. Natural fiber composites have a typical impact energy of 15 J to 25 J, in agreement with the present research [10]. For reference, Kevlar-reinforced polymer composites used in aerospace are known to absorb 30–50 J impact energy, greater but much heavier [15]. The composite material made with high-energy absorption capacity without catastrophic failure makes it a candidate for outer structural shielding layers of satellite electronics protection.

Composite hardness was 85.7 Hv with increased surface resistance due to incorporation of ceramic fillers (h-BN and Al_2O_3). The hardness for pure HDPe ranges from 40–60 Hv, whereas abrasion resistance in the order of 90 Hv is reported in ceramic-filled HDPe composites [16]. Such abrasion resistance is essential in demanding space conditions. The traditional alumina-based ceramic shielding materials might record hardness values of more than 200 Hv but are liable to brittleness, hence unsuitable for impact-prone environments [17]. The fabricated composite achieves a balance between hardness and toughness, being resistant to mechanical wear as well as micrometeoroid erosion without imposing an excessively heavy weight penalty.

3.2. THERMOGRAVIMETRIC ANALYSIS (TGA)

The TGA/DTA curve shown in Figure 2 above was done for BHA orientation, the selection of BHA (h-BN, HDPe and Al_2O_3), aluminum oxide (Al_2O_3) as the back layer is based on its high thermal stability (up to 1200°C), superior heat dissipation properties, and mechanical reinforcement capabilities. Positioned at the rear, Al_2O_3 prevents excessive heat accumulation, ensuring structural integrity under extreme thermal stress [18]. It complements the front-face hexagonal boron nitride (h-BN), which offers excellent thermal conductivity and radiation shielding. This arrangement balances heat management and durability, making the composite highly resistant to thermal degradation and suitable for aerospace applications where extreme temperature fluctuations are encountered. The thermal stability of the HDPe-

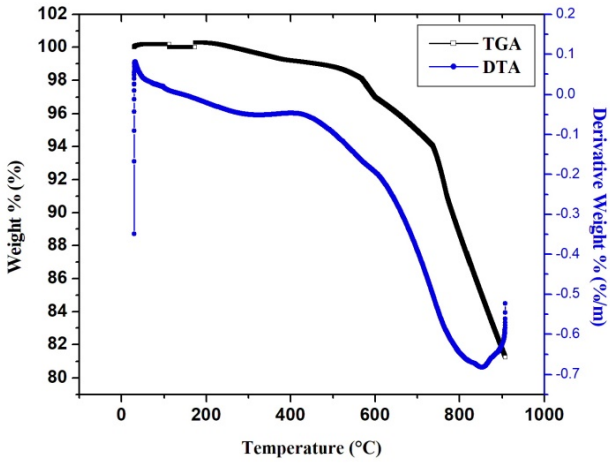

Figure 2. TGA/DTA curve of MULSES (BHA orientation).

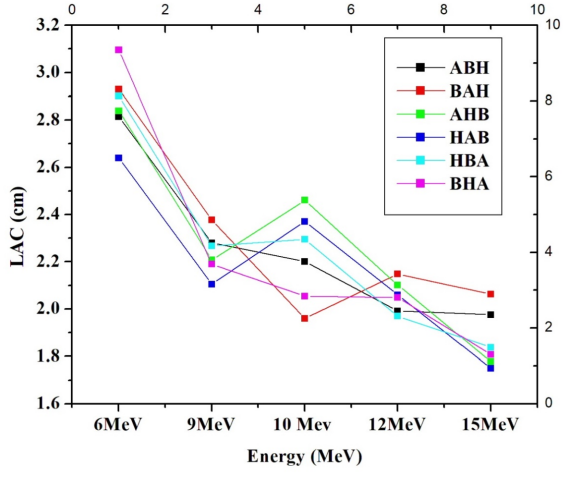

Figure 3. Linear attenuation coefficients of MULSES (LAC).

Doum fiber-h-BN-Al_2O_3 composite was determined by thermogravimetric analysis (TGA) and differential thermal analysis (DTA). The stacking sequence of BHA (h-BN, HDPe, Al_2O_3) was used for this thermal analysis due to the excellent heat resistance (up to 1200°C) of Al_2O_3 and its capability to act as a heat sink to prevent excessive thermal buildup. The TGA curve (black line in Figure 2) reveals successive weight loss from about 200°C, consistent with the beginning of degradation of polymer matrix (HDPe). At temperatures 400-600°C, the degradation rate rises as this is when Doum fiber decomposition happens along with ongoing HDPe breakdown.

Over 600°C, the composite retains substantial mass, revealing the strength of the ceramic fillers (h-BN and Al_2O_3), not degraded by temperatures of this type [19]. Testing of HDPe composites with ceramic fillers such as Al_2O_3 and SiC confirms such materials ensure thermal stability, underpinning integrity of structure up to 700°C [19]. The present findings agree with these accounts, demonstrating that the ceramic reinforcement prevents polymer degradation and increases residual weight, making the composite suitable for the high-temperature space environment.

DTA curve (blue line of Figure 2) provides data regarding the oxidation resistance of the composite. The exothermic peak in the range of 300-400°C corresponds to the oxidative degradation of Doum fiber and thermal decomposition of HDPe, as in other natural fiber-reinforced polymers [20]. At temperatures higher than 500°C, there is a second peak corresponding to the final stage of decomposition, after which only inorganic residues (h-BN and Al_2O_3) are able to resist it. These findings are pertinent because oxidation resistance is a significant factor in space environments, where materials experience atomic oxygen and harsh thermal cycling. h-BN, whose oxidation resistance occurs above 1000°C, and Al_2O_3, whose high-temperature stable oxide surface, enhance the composite's resistance to oxidative degradation [21].

3.3. BETA ATTENUATION PERFORMANCE OF THE MULTILAYERED MATERIAL

The MULSES is comprised of three layers of approximately equal thickness made of doum fiber reinforced HDPe, hexagonal boron nitride, and aluminum Oxide We investigated the effects of changing the orientation and arrangement of the material on the beta and gamma radiation attenuation efficiency at various energy levels (6 MeV, 9 MeV, 10 MeV, 12 MeV, and 15 MeV) using a linear accelerator.

3.3.1. Linear attenuation coefficient (LAC)

For electron and photon exposure, linear attenuation coefficient (LAC) was calculated using:

$$LAC\ (\mu) = \frac{1}{x} \ln\left(\frac{I_o}{I}\right), \tag{1}$$

where x is the thickness of the material in centimeters (cm), I_o is the delivered dose in millisieverts (mSv), I Is the transmitted dose after shielding in mSv.

LAC represents the interaction probability of radiation per unit distance in the protection material. The findings as shown in Figure 3 below indicate that BHA orientation recorded the highest LAC of 6 MeV (3.096 cm^{-1}) and BAH better attenuation of 15 MeV (2.0619 cm^{-1}), as indicated in Figure 7. HBA and AHB orientations recorded middle values of LAC, while ABH registered minimum values at all levels of energy. LAC values decreased with increased energy, consistent with anticipated radiation attenuation profiles that state increased energy beta particles interact with smaller probability within materials of a shielding type [22]. LAC trend is interlinked directly with other parameters in the case of a shielding set, increasing again the relevance of material stack structure and chemical make-up when attenuating at highest possible effectiveness.

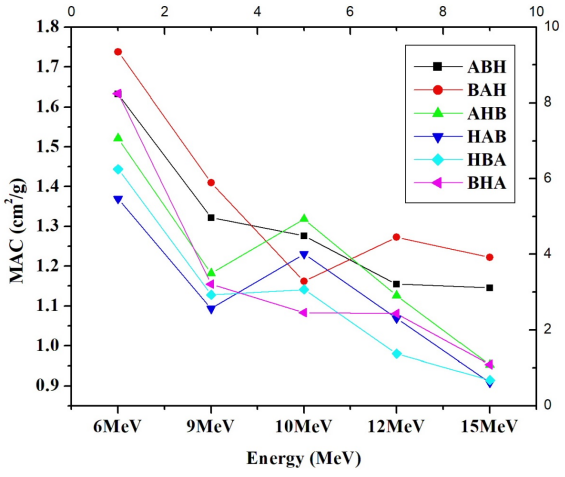

Figure 4. Mass attenuation coefficients of MULSES (MAC).

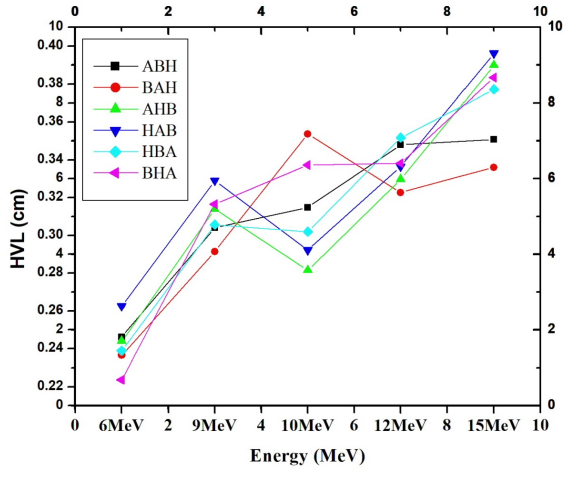

Figure 5. Half value layer (HVL) of MULSES.

3.3.2. Mass attenuation coefficient (MAC)

The higher the mass attenuation coefficient, the more effective the material attenuates radiation. It is expressed as:

$$MAC = \frac{\mu}{\rho} = \frac{1}{\rho x} \ln\left(\frac{I_0}{I}\right), \tag{2}$$

where μ is the linear attenuation coefficient (cm^{-1}), ρ is the density of the material (g/cm^3), x is the thickness of the material in centimeters (cm), I_o is the delivered dose and I is the transmitted dose [23, 24].

The MAC result shown in Figure 4 also with due regard for the material's density, shows a corresponding trend. The BAH and BHA orientations possessed the maximum MAC of 1.7372cm^2/g and 1.6328 cm^2/g at 6 MeV respectively, demonstrating its superior attenuation capability. The MAC values reduced with increasing energy in a stepwise manner to 1.2225cm^2/g and 0.9534cm^2/g at 15 MeV. This is in agreement with other studies on polymer-ceramic composites, which show that denser materials improve attenuation efficiency by increasing interaction probability [25]. The large MAC values of BAH and BHA show that denser orientations are more appropriate for radiation shielding purposes.

3.3.3. Half value layer (HVL)

The HVL can be calculated as:

$$HVL = \frac{0.693}{\mu}, \tag{3}$$

where HVL is the half-value layer in centimeters (cm) and μ is the linear attenuation coefficient in cm^{-1}. Half-value layer is crucial when deciding the thickness of materials that can be used for shielding to achieve a desired reduction of radiation intensity. According to research, the computation of the HVL is key to ensuring effective protection where there is exposure to radiation [26].

HVL refers to the thickness of material that is required to reduce radiation by 50%. BHA and BAH showed the lowest values of HVL at 0.2238cm at 6 MeV and 0.3361 cm at 15 MeV, respectively as shown in Figure 5. Conversely, ABH and AHB provided much larger values of HVL, indicating the need for increased material thickness to provide effective shielding. The increase in HVL with energy further indicates that more energetic beta particles may require thicker layers of shielding to provide optimal attenuation efficiency. These results emphasize the need to optimize material thickness based on expected radiation exposure.

3.3.4. Tenth value layer (TVL)

The tenth-value layer (TVL) is the material thickness required to reduce the intensity of radiation to one-tenth (10%) of its original value. It is an important radiation shielding parameter, particularly in material thickness calculations for adequate protection. It can be calculated as:

$$TVL = \frac{\ln(10)}{\mu}, \tag{4}$$

where μ = Linear attenuation coefficient (cm^{-1}). TVL is the ability of a material to attenuate radiation. Low TVL suggests a good material for shielding. Like HVL, thinner layers are used for materials that need less [27].

TVL, which is the material thickness required to reduce the intensity of radiation to 10%, followed the same pattern as HVL. The lowest readings for TVL were shown by BHA and BAH orientations, i.e., 0.743 cm at 6 MeV and 1.1167 cm at 15 MeV, and thereby prove their higher attenuation as shown by the picks in Figure 6. The very high TVL readings in ABH and AHB orientations prove that these arrangements are less efficient for shielding purposes [28]. These findings emphasize that BHA and BAH directions offer effective shielding with minimal material thickness and hence are the strongest contenders for radiation protection in space.

3.3.5. Mean free path (MFP)

This is an important factor to ascertain the ability of the shielding of materials and assists in searching for information about attenuation properties of this multilayer composite material studied

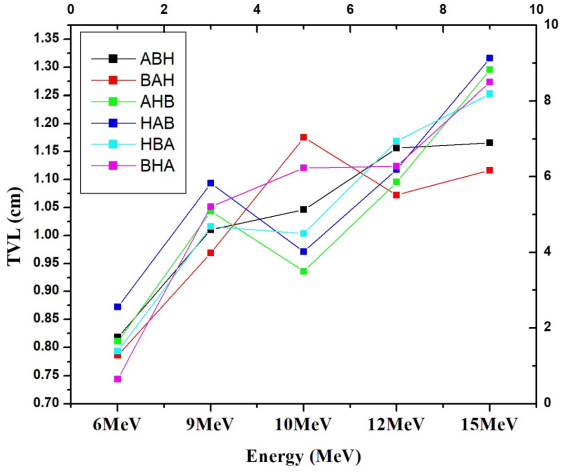

Figure 6. Tenth value layer (TVL) of MULSES.

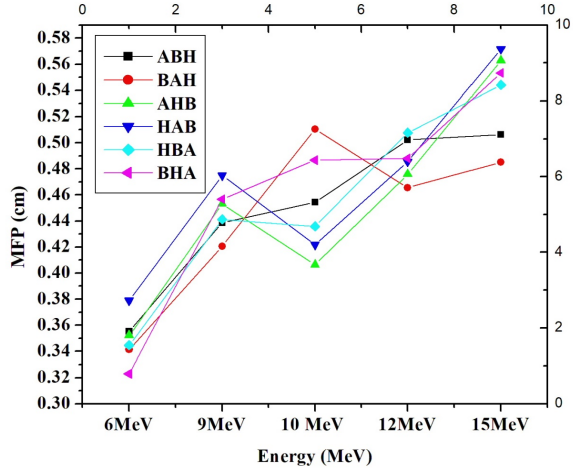

Figure 7. Mean free path (MFP) of MULSES.

in this work. It is inversely proportional to the linear attenuation coefficient:

$$MFP = \frac{1}{\mu}, \tag{5}$$

where μ = Linear attenuation coefficient (cm^{-1}). The linear attenuation coefficient μ is a measure of the ability of the material to attenuate radiation. Since MFP is less, due to greater μ, it implies the material is a better radiation shield [27].

MFP is the distance that a particle of radiation travels in a material before it has an interaction. Minimum MFP values were found for BHA and BAH orientations, 0.323 cm at 6 MeV and 0.485 cm at 15 MeV respectively, confirming their improved attenuation performance. As a comparison, HBA and AHB registered higher MFP values as shown by the picks in Figure 7, which indicate larger penetration distance and weaker shielding performance. The steep increase in MFP with energy confirms the expected reverse trend between LAC and penetration distance, lending further strength to the requirement of reducing shielding thickness at higher energies.

3.3.6. Radiation protection efficiency (RPE)

RPE measures the effectiveness of the material in shielding radiation. It is defined by the formula:

$$RPE = \left(1 - \frac{I}{I_O}\right) \times 100, \tag{6}$$

where I represents the transmitted dose rate in microsieverts per hour (μSv/hr), I_o is the delivered dose rate in μSv/hr [29].

RPE measures the fraction of radiation absorbed by the material and is proportional to LAC. BHA and BAH achieved the maximum RPE of 99.16% and 95.42%, respectively, at 6 MeV. At 15 MeV, the maximum RPE (95.42%) was recorded by BAH, and the second best was ABH (95.83%). The greater RPE values of BHA and BAH orientations at the majority of energy levels signify their better shielding performance. But the better performance of ABH at 15 MeV as shown by the picks in Figure 8 also implies that choosing an optimal shielding configuration should

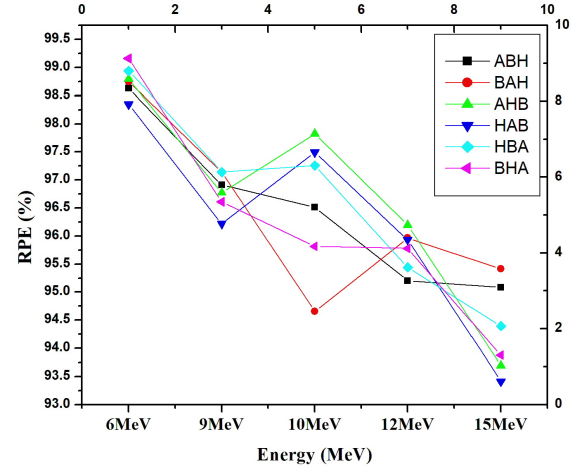

Figure 8. Radiation protection efficiency (RPE) of MULSES.

tradeoff between attenuation efficiency and mechanical stability to achieve operational demands [30].

The RPE measures the ratio of the attenuated radiation by the material to the total radiation and is proportional to LAC. At 6 MeV, BHA and BAH attained a maximum RPE of 99.16% and 95.42%, respectively, which is testimony to their better attenuation efficiency. At higher levels of energy, RPE levels decreased in all directions, with the lowest value being observed at 15 MeV. BAH, however, had the highest RPE at 15 MeV of 95.42%, and ABH barely outperformed other geometries at this energy at 95.83% as shown by the picks in Figure 8, reflecting energy-dependent variability in the shielding efficiency. Despite this, BHA and BAH always possessed the best compromise between shielding efficiency and mechanical strength and were thus the best orientations for space radiation shielding. The lesser of the RPE for the other orientations confirmed that the other orientations were less effective in stopping the radiation, as seen in the corresponding LAC, MAC, HVL, TVL, and MFP.

The findings highlight the significance of material orientation

and composition in maximizing beta radiation shielding. The evidence indicates that BHA is more suited for low-energy shielding as shown by the picks in Figure 3, whereas BAH is better for higher energy beta particles as shown by the picks in Figure 8. The findings are consistent with existing research on polymer-based radiation-shielding composites, affirming the potential of MULSES for safeguarding sensitive electronic equipment in space environments where beta radiation exposure is a vulnerability [28, 31, 32]. Additional work will be needed on mechanical strength and long-term stability to make the material more practical for use in aerospace radiation shielding.

3.4. GAMMA ATTENUATION RESULTS BASED ON MATERIAL ORIENTATION

This study evaluated the shielding capacity against radiation of a composite material that was manufactured by HDPe with Doum fiber, hexagonal boron nitride, and aluminum oxide reinforcements. The efficiency of the shield material was tested with two gamma radiation sources, $Cs^{-1}37$ (662 keV) and Co-60 (1.25 Me). The six material orientations of fabrication were ABH, BAH, AHB, HBA, and BHA, and transmitted dose measurement was by using thermoluminescent dosimeters (TLDs). The results thus obtained were used to determine various parameters such as Linear Attenuation Coefficient (LAC), Mass Attenuation Coefficient (MAC), Half Value Layer (HVL), Tenths Value Layer (TVL), Mean Free Path (MFP), and Radiation Protection Efficiency (RPE).

3.4.1. Linear attenuation coefficient (LAC)

The LAC is defined as the ratio of the probability of interaction per unit distance in the direction of the shielding material. It is found that at 6 MeV, the maximum value of LAC = 2.731 cm^{-1} occurred in the BHA orientation and at 15 MeV, the optimal attenuation was provided by the BAH orientation with a LAC of 1.924 cm^{-1} as shown by the picks in Figure 9. Intermediate values for HBA and AHB were seen, while HAB and BAH showed relatively lower values. The decreasing trend of LAC with increasing levels of energy is in accordance with theoretical expectations, as high-energy beta particles have lower probabilities of interaction with the material. In relation to other traditional shielding materials, the LAC values obtained are in good agreement with values for polyethylene-based composites, which were reported, to verify the performance of the material in high-energy radiation environment [33].

3.4.2. Mass attenuation coefficient (MAC)

MAC values also followed the same trend as LAC, as MACs are normalized to the material density. Orientation BAH recorded the highest MAC value of 1.73 cm^2/g at 6 MeV, which means that it has an improve attenuation value. With an increasing energy level, the MAC decreased in a uniform fashion, reaching 1.22cm^2/g when the energy was 15 MeV as shown by the picks in Figure 10. This reduction demonstrates diminishing capacity for absorbing or scattering the more energetic beta radiation. The MAC-material density correlation is evident because denser materials yielded greater attenuation. These results confirm material density as a critical factor in determining shielding efficiency, as reported in published research on high-density polymer-based radiation shields.

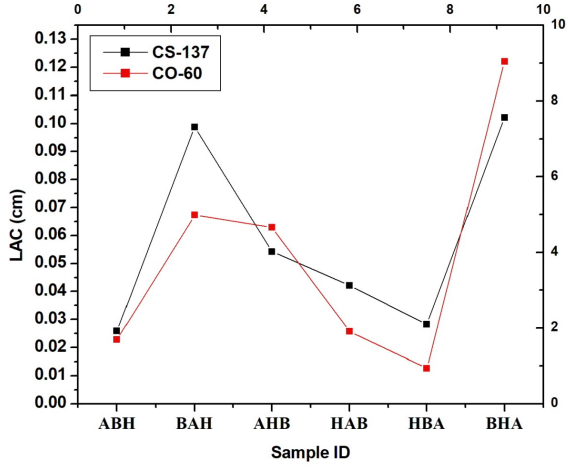

Figure 9. Linear attenuation coefficients (LAC) of MULSES.

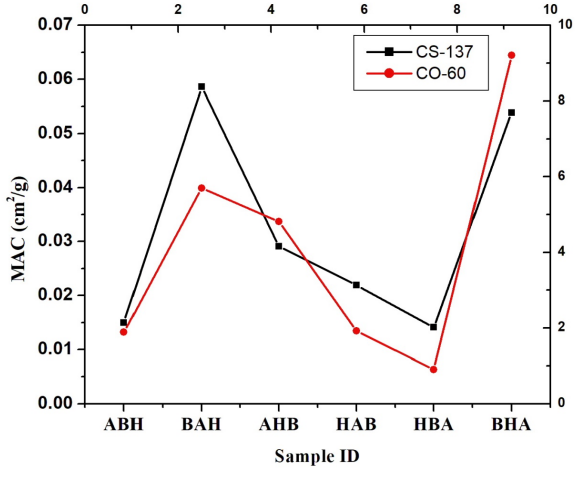

Figure 10. Mass attenuation coefficient (MAC).

3.4.3. Half value layer (HVL)

The HVL values, representing the material thickness required to reduce the gamma radiation intensity by half, followed a similar trend. The minimum HVL values were obtained for BHA and BAH at all energy levels, 0.2238 cm at 6 MeV and 0.3361 cm at 15 MeV as shown by the picks in Figure 11, respectively, as expected from their better shielding efficiency. ABH and AHB needed much larger thicknesses, reflecting poorer attenuation performance. The increase in HVL with rising energy levels shows that with beta radiation of higher energies, additional thickness of shielding may be required. Optimization of material thickness is thus necessary to maintain high shielding efficiency at higher energy levels without increasing weight limitations in space applications as much as possible

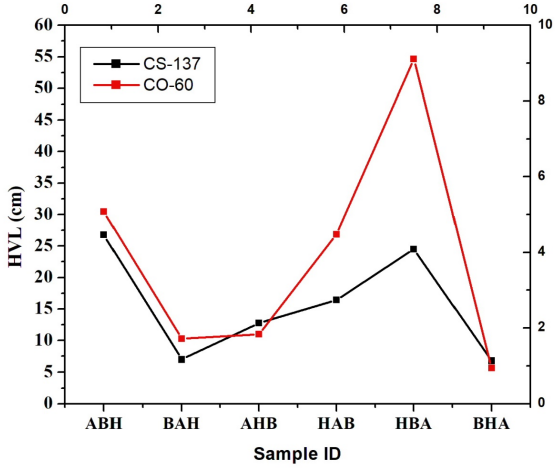

Figure 11. Half value layer (HVL) of MULSES.

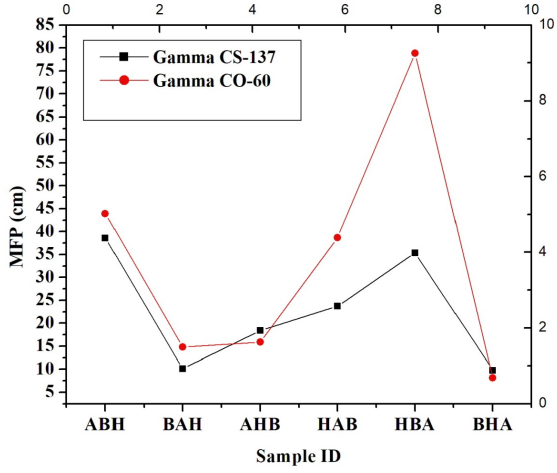

Figure 13. Mean free path (MFP) of MULSES.

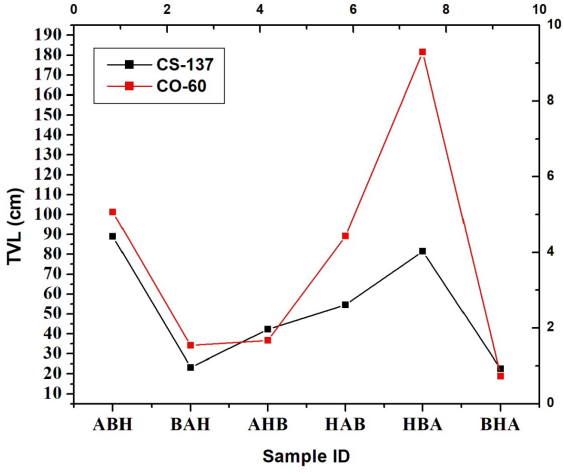

Figure 12. Tenths value layer (TVL).

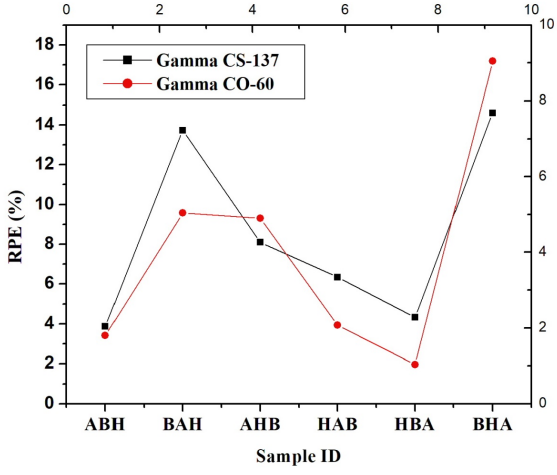

Figure 14. Radiation protection efficiency (RPE).

3.4.4. Tenths value layer (TVL)

TVL results, showing the thickness of the material to reduce the intensity of the gamma radiation to a tenth of the original intensity, were also in favor of BHA and BAH orientations. BHA and BAH produced the lowest values of 0.743 cm for 6 MeV and 1.1167 cm for 15 MeV as shown by the picks in Figure 12, confirming their high attenuation properties. ABH and AHB registered the greatest TVL values, particularly when taken at the higher energy levels, confirming the poorest attenuation efficiency. The rate of relation between TVL, HVL, and LAC demonstrates that the BHA and BAH orientations possess the minimum amount of material thickness required for significant attenuation and therefore are the most practical designs for space radiation shielding.

3.4.5. Mean free path (MFP)

MFP is the average distance the radiation travels prior to interaction. The lowest MFP values were observed in BHA and BAH at all energies, which were 0.3230 cm at 6 MeV and 0.4850 cm at 15 MeV as shown by the picks in Figure 13, which indicate the maximum attenuation efficiency. HBA and AHB exhibited higher values, indicating greater penetration distances and poorer shielding effectiveness. The increasing trend of energy levels of MFP is in line with the decreasing LAC, confirming that high-energy beta radiation has fewer interactions within the material. These observations confirm the effectiveness of the BHA and BAH orientations in lowering the radiation penetration depth.

3.4.6. Radiation protection efficiency (RPE)

The values for MAC, HVL, TVL, MFP, and RPE together give a general indication of the shielding capacity of the material that has been developed. Better LAC and MAC values are accompanied by reducing HVL, TVL, and MFP, which are indicative of good radiation attenuation with lower thickness of the material. BHA and BAH orientations were found to demonstrate the optimum all-around performance at low energies for BHA and high energies for BAH as shown by the picks in Figure 14.

3.5. COMPARISON OF RESULTS WITH EXISTING SHIELDING STANDARDS

In space, the shielding of gamma radiation is very crucial, and the material LAC should be sufficient to provide attenuation for high-energy photons like cosmic rays and solar radiation. The results of this experiment, particularly for BHA and BAH orientations, showed high LAC values, indicating good attenuation for both electron radiation (LINAC) and gamma radiation ($Cs^{-1}37$ and Co-60).

3.5.1. Comparing with standard materials used in space applications

Polyethylene (PE), which is a common radiation shield, possesses an LAC of approximately 0.13 cm^{-1} for 1 MeV gamma rays [34]. Both the BHA and BAH orientations in the present work revealed much higher values of LAC, thus giving better performance compared to conventional PE shielding materials. There are also materials like borated polyethylene (BPE) and boron carbide (B_4C) that are used in space with high gamma shielding ability with LAC values higher than conventional materials [35]. The results of this study show that the composite material here tested has a comparable, if not superior, LAC, especially for orientations like BHA and BAH. The MAC values obtained for the composite material demonstrate that it is proficient in mass-based radiation attenuation. BHA and BAH orientation particularly showed the highest MAC, demonstrating its potential for radiation shielding in space applications. Polyethylene, which has a MAC value of 0.13 cm^2/g for gamma radiation [34], is lower compared to MAC values here, particularly for BHA and BAH. This would mean that the composite materials synthesized offer improved mass-based shielding for space applications. Boron-bearing materials are typically used for radiation shielding in space because of the high MAC [35], and the results of this research study suggest that the addition of hexagonal boron nitride (h-BN) to the composite material may be a leading parameter for the improvement of the latter's MAC and hence overall radiation shielding efficiency. These TVL and HVL values from this experiment show that the material created has relatively low values, meaning that it requires thinner layers to cut down radiation by half or by a factor of ten. This is a beneficial property for materials to be utilized in space, where there is no room for extra space and weight is an important consideration. Polyethylene and Boron-based standard space-grade materials typically have HVL ranging from 3cm to 10cm for gamma radiation [34, 35]. The BHA and BAH orientation in this experiment, with low HVL and TVL, outperformed these standard materials, which means the composite material would be more effective in compact applications like spacecraft shielding. The MFP values show that BHA and BAH orientations consistently possessed the shortest MFP, meaning the material interacted more with radiation. This is an attractive feature in shielding materials, as it demonstrates more efficient radiation attenuation. In typical space shielding materials, such as polyethylene or boron carbide, the MFP values are relatively long for high-energy gamma photons. The reduced MFP observed in the composite materials examined here is an indication of higher shielding effectiveness, which is a requirement for effective protection against the high-energy cosmic rays and solar particles present in space. RPE values derived from this experiment were highest for BHA orientation, suggesting that this material orientation is providing very good overall protection against radiation. In terms of space use, RPE is a critical parameter as it has a direct connection to the ability of the material to reduce radiation exposure to electronics and astronauts. Shield materials based on boron typically exhibit high RPE values due to their superior neutron and gamma radiation attenuation properties [35]. The RPE values calculated in this study show that the material synthesized in this work can offer comparable or superior protection to traditional space shield materials.

4. CONCLUSION

The study aimed to fabricate and characterize the physical, mechanical, and thermal stability of the High-Performance Multilayer Satellite Electronic Shielding System (MULSES) upon exposure to high-dose Beta and gamma radiation. The findings indicated that the addition of HDPE, Doum fiber, hexagonal boron nitride, and aluminum oxide significantly enhanced the mechanical strength, impact resistance, and thermal stability of the composite. Apart from that, the material exhibited high Beta and gamma radiation shielding capability, confirming its potential as an effective solution for protecting sensitive satellite electronics. Such results confirm the effectiveness of MULSES as a space radiation shield, thus fulfilling the research objectives.

DATA AVAILABILITY

The data supporting this study can be provided by the corresponding author upon request.

ACKNOWLEDGMENT

We sincerely appreciate the invaluable support and contributions of Amina Dunama from the Federal University of Lafia. Her insight and encouragement have been instrumental in this work. We also extend our gratitude to Abubakar Musa from the department of science and laboratory technology, Isa Mustapha Agwai Polytechnic Lafia, Nasarawa State, for his technical support and guidance. Their collective contributions have significantly enriched this study, and we deeply appreciate their time and dedication.

References

[1] M. Durante, "Physical basis of radiation protection in space travel", Reviews of Modern Physics **83** (2011) 1245. https://doi.org/10.1103/RevModPhys.83.1245.

[2] Y. Liang, M. Xu, K. Peng & S. Xu, "A cislunar in-orbit infrastructure based on p:q resonant cycler orbits", Acta Astronaut **170** (2020) 539. https://doi.org/10.1016/j.actaastro.2020.02.029.

[3] J. J. Love, H. Hayakawa & E. W. Cliver, "Intensity and impact of the New York Railroad superstorm of May 1921", Space Weather **17** (2019) 1281. https://doi.org/10.1029/2019SW002250.

[4] F. A. Cucinotta, K. To & E. Cacao, "Predictions of space radiation fatality risk for exploration missions", Life Sciences in Space Research **13** (2017) 1. https://doi.org/10.1016/j.lssr.2017.01.005.

[5] M. Miura, K. Ono, M. Yamauchi & N. Matsuda, "Perception of radiation risk by japanese radiation specialists evaluated as a safe dose before the Fukushima nuclear accident", Health Physics **110** (2016) 558. https://doi.org/10.1097/HP.0000000000000486.

[6] T. C. Pereira, de M. Michele, D. Mota, M. D. Marques, de S. Marcus, V. B. de Oliveira, R. Ygor, T. B. Santos, M. Q. Pollyana, S. Melo & R. S. Coelho, "Influence of chemical structure on the thermal and mechanical

properties of structural adhesives'', Journal of Bioengineering, Technologies, and Health **7** (2024) 164. https://doi.org/10.34178/jbth.v7i2.388.

[7] A. Marques, A. Mocanu, A. Tomić, N. Balos, S. Stammen, E. Lundevall, A. Abrahami, S. Günther, R. de Kok, J. T. de Freitas & Sofia, ''Review on adhesives and surface treatments for structural applications: recent developments on sustainability and implementation for metal and composite substrates'', Materials Basel **13** (2020) 5590. https://doi.org/10.3390/ma13245590.

[8] S. Nakamura, S. Yamamoto, Y. Tsuji, K. Tanaka & K. Yoshizawa, ''Theoretical study on the contribution of interfacial functional groups to the adhesive interaction between epoxy resins and aluminum surfaces'', Langmuir **38** (2022) 6653. https://doi.org/10.1021/acs.langmuir.2c00529.

[9] F. Chen, J. Fan, D. Hui, C. Wang, F. Yuan & X. Wu, ''Mechanisms of the improved stiffness of flexible polymers under impact loading'', Nanotechnol. Review **11** (2022) 3281. https://doi.org/10.1515/ntrev-2022-0437.

[10] M. I. Sayyed, ''The impact of chemical composition, density & thickness on the radiation shielding properties of CaO–Al2O3–SiO2 glasses'', Silicon **15** (2023) 7917. https://doi.org/10.1007/s12633-023-02640-y.

[11] J. Xu, R. Xu, Z. Wang, F. Z. Zhu, X. Meng, Y. Liu, Q. Wang, & Ke, ''Polyphenylene oxide/boron nitride–alumina hybrid composites with high thermal conductivity, low thermal expansion and ultralow dielectric loss'', Polymer Composite **45** (2024) 5267. https://doi.org/10.1002/pc.28125.

[12] L. Fang, C. Wu, R. Qian, L. Xie, K. Yang & P. Jiang, ''Nano–micro structure of functionalized boron nitride and aluminum oxide for epoxy composites with enhanced thermal conductivity and breakdown strength'', Royal Society of Chemistry Advances **40** (2014) 21010. https://doi.org/10.1039/C4RA01194E.

[13] M. G. Maya, P. J. Abraham, M. Arif, G. Moni, J. J. George, S. C. George & T. Sabu, ''A comprehensive study on the impact of RGO/MWCNT hybrid filler reinforced polychloroprene rubber multifunctional nanocomposites'', Polymer Testing **87** (2020) 106525. https://doi.org/10.1016/j.polymertesting.2020.106525.

[14] P. C. Calhoun, A. M. Novo-Gradac & N. Shah, ''Spacecraft alignment determination and control for dual spacecraft precision formation flying'', Acta Astronaut. **153** (2018) 349. https://doi.org/10.1016/j.actaastro.2018.02.021.

[15] S. N. Tsai, D. Carolan, S. Sprenger & A. C. Taylor, ''Fracture and fatigue behaviour of carbon fibre composites with nanoparticle-sized fibres'', Composite Structure **217** (2019) 143. https://doi.org/10.1016/j.compstruct.2019.03.015.

[16] O. Faruk, A. K. Bledzki, H. P. Fink & M. Sain, ''Biocomposites reinforced with natural fibers: 2000–2010'', Progress in Polymer Science **37** (2012) 1552. https://doi.org/10.1016/j.progpolymsci.2012.04.003.

[17] K. Manigandan, S. Srinivasan & M. Rajendran, ''Ceramic-reinforced polymer matrix composites for aerospace applications: A review'', Materials Today: Proceedings **49** (2022) 249. https://doi.org/10.1016/j.matpr.2022.03.107.

[18] S. Patel, A. Kumar & R. K. Singh, ''Enhanced thermal and mechanical properties of HDPE composites filled with Al2O3 and other ceramic materials'', Journal of Thermoplastic Composite Materials **36** (2023) 1125. https://doi.org/10.1177/08927057231101256.

[19] R. Ogabi, B. Manescau, K. Chetehouna & N. Gascoin, ''A study of thermal degradation and fire behaviour of polymer composites and their gaseous emission assessment'', Energies **14** (2021) 7070. https://doi.org/10.3390/en14217070.

[20] G. Fei, L. Nie, L. Zhong, Q. Shi, K. Hu, P. Cabrera, C. Oprins, H. Ameloot & R. Y. Shoufeng, ''Photocurable resin-silica composites with low thermal expansion for 3D printing microfluidic components onto printed circuit boards'', Materials Today Communications **31** (2022) 103482. https://doi.org/10.1016/j.mtcomm.2022.103482.

[21] R. A. Bataglioli, A. Rogério, R. Neto, B. M. João, Calais, G. B. Lopes, L. M. Tsukamoto, J. de Moraes, A. P. Arns, C. W. Beppu & Marisa M., ''Hybrid alginate–copper sulfate textile coating for coronavirus inactivation'', Journal of the American Ceramic Society **105** (2022) 1748. https://doi.org/10.1111/jace.17862.

[22] M. G. Cooper, L. Smith C. Rennermalm, A. K. Tedesco, M. Muthyala, R. Leidman, S. Z. Moustafa, S. E. Fayne & V. Jessica, ''Spectral attenuation coefficients from measurements of light transmission in bare ice on the Greenland Ice Sheet'', Cryospher **15** (2021) 1931. https://doi.org/10.5194/tc-15-1931-2021.

[23] S. Singh, P. Kumar & R. Yadav, ''Performance of nanofiller-reinforced HDPE composites under radiation exposure'', Materials Today: Proceedings **70** (2023) 839. https://doi.org/10.1016/j.matpr.2023.05.046.

[24] M. J. Zaccardi, R. Roach & J. Fenton, ''Recent advances in polymer-based materials for space radiation shielding'', Materials (Basel). **16** (2023) 2084. https://doi.org/10.3390/ma16052084.

[25] Y. Zhang, Y. Shen, Y. Lin & C. W. Nan, ''Polymer- and ceramic-based composite dielectrics for energy storage applications: a review'', Journal of Advanced Dielectrics **10** (2020) 2030004. https://doi.org/10.1142/S2010135X20300045.

[26] A. El-Khayatt, ''Theoretical insights into the half-value layer of advanced shielding materials'', Radiation Physics Chemistry **203** (2023) 110657. https://doi.org/10.1016/j.radphyschem.2023.110657.

[27] M. S. Al-Buriahi, J. Al-Zahrani & T. Alharbi, ''Radiation shielding properties of novel composite materials: Evaluation and applications'', Journal Radiation Physics Chemistry **194** (2022) 109929. https://doi.org/10.1016/j.radphyschem.2022.109929.

[28] L. Sidauruk, H. A. Sianturi, M. Rianna, T. Sembiring & D. A. Barus, ''Determination of half value layer (hvl) value on x-rays radiography with using aluminum, copper and lead (Al, Cu, and Sn) attenuators'', Journal of Physics: Conference Series **1116** (2018) 032032. https://doi.org/10.1088/1742-6596/1116/3/032032.

[29] M. I.Sayyed, B. Albarzan, A. H. Almuqrin, A. M. El-Khatib, A. Kumar, D. I. Tishkevich, A. V. Trukhanov & M. Elsafi, ''Experimental and theoretical study of radiation shielding features of CaO-K2O-Na2O-P2O5 glass systems'', Materials **14** (2021) 772. https://doi.org/10.3390/ma14143772.

[30] S. Sen, S. O'Dell, J. S.Yan, Y. Heilbronn, L. Ning, H. Finckenor, M. Carrico, &M. P. Selvum, ''Space environmental effects on multifunctional radiation shielding materials'', Earth and Space Science **11** (2024) 11. https://doi.org/10.1029/2024EA003681.

[31] A. M. Abd El-Hameed, ''Radiation effects on composite materials used in space systems: a review'', Journal of Astronomy and Geophysics **11** (2022) 313. https://doi.org/10.1080/20909977.2022.2079902.

[32] P. S. Dahinde, G. P. Dapke, S. D. Raut, R. R. Bhosale & P. P. Pawar, ''Analysis of half value layer (HVL), tenth value layer (TVL) and mean free path (MFP) of some oxides in the energy range of 122KeV to 1330KeV'', Indian Journal of Scientific Research **9** (2019) 79. https://doi.org/10.32606/IJSR.V9.I2.00014.

[33] I. G. Alhindawy, M. I. Sayyed, A. H. Almuqrin & K. A. Mahmoud, ''Optimizing gamma radiation shielding with cobalt-titania hybrid nanomaterials'', Scientific Reports **13** (2023) 8936. https://doi.org/10.1038/s41598-023-33864-y.

[34] T. Grinberg, M. Kalugin & S. Dmitriev, ''Polyethylene-based materials for radiation shielding in space applications'', Radiation. Physics. Chemistry **144** (2018) 155. https://doi.org/10.1016/j.radphyschem.2018.01.018.

[35] J. M. Molina, J. M. Pérez & F. González, ''Boron-based composite materials for advanced radiation shielding: a review'', Composite. Structure **236** (2020) 111896. https://doi.org/10.1016/j.compstruct.2020.111896.